https://doi.org/10.1038/s44406-026-00019-7

Towards resilient renewable energy deployment in Africa through a weather-aware optimization framework

Rajeev Sukumara Kurup[1], Hannah C Bloomfield[2], P. R. Tiwari[1] ✉, Nachiketa Acharya[3] & Evelyn Hesse[1]

Renewable energy deployment in Africa must account for the continent's pronounced weather variability to ensure a reliable electricity supply. Here, we introduce a weather-aware framework that integrates multi-criteria decision analysis with assessments of meteorological variability to optimize renewable site selection. Optimal solar and wind energy locations are identified not only by their highest average yields but also by evaluating generation variability under major climate oscillations, including the Madden–Julian Oscillation modulated by El Niño–Southern Oscillation. In addition, novel synoptic regimes are derived through self-organizing map cluster analysis, providing further insight into region-specific drivers of variability. Country-level yield estimates reveal the dominant meteorological patterns shaping renewable output and their frequencies of occurrence. Our findings underscore the necessity of accurately forecasting these regimes to enhance system resilience and inform long-term planning. By explicitly linking generation variability to underlying climate drivers, this framework offers a robust pathway for optimizing renewable energy expansion across Africa.

Africa's energy demand is projected to triple over the coming decades[1], positioning renewable energy (RE) as central to the continent's power strategy. Hydropower has historically underpinned African RE portfolios[2], yet rapid cost declines in wind and solar technologies[3,4] paired with the imperative to conserve freshwater are expected to accelerate progress towards the Sustainable Africa Scenario (SAS) goals[5] by 2030. If all currently proposed projects were implemented, RE could satisfy 76% of Africa's projected 2040 electricity demand, with solar and wind providing the dominant shares[6]. Realizing this outcome requires strategic planning that integrates infrastructure readiness, resource distributions, and the impacts of weather and climate variability[7].

Africa's renewable energy potential is vast. Continental assessments indicate roughly 110 GW of developable wind capacity and about 10 TW of solar potential[8]. Solar prospects are especially strong because nearly 90% of the landmass receives substantial incoming solar radiation[9]; however, production remains sensitive to high cloud cover, dust aerosols, and temperature[10]. Favorable locations for wind power generation have been identified in North and Southern Africa, the Horn of Africa, and coastal regions[11,12]. However, key geospatial considerations for RE deployment include existing grid infrastructure, population density, and geographical constraints[1]. Identifying optimal deployment sites for wind and solar power, such as the model supply regions (MSRs) defined by Sterl et al.[13] improves the effectiveness of energy planning. RE sources are subject to intrinsic variability of the natural weather systems[14], therefore, a thorough understanding of the local meteorology, large-scale synoptic circulation features, and the impacts of global teleconnections is essential for operations from days to decades ahead[15,16].

Among the numerous synoptic features that constitute the day-to-day to sub-seasonal meteorological variability over Africa (affecting RE production and demand) are weather regimes[17]. Weather regimes can be defined as large-scale recurring patterns in the atmospheric circulation, which can persist for periods from days to weeks[18,19]. Much has been done to investigate their impacts on energy production over Europe, where renewable generation tends to be above normal in the presence of cyclonic weather patterns (particularly in wind dominated systems) but below normal during blocked-regimes[20–23]. Concurrently, energy demand rises during blocked regimes, emphasizing the interconnectedness between climate variability and present-day energy systems. Bloomfield et al.[23] developed a new approach to defining weather regimes called "targeted circulation types" (TCTs) where the patterns were defined by clustering continental-scale energy variables and showed that the resultant four TCTs explain European power system variability better than standard weather regimes. These new circulation types retain the sub-seasonal predictability of traditional weather regimes while being more directly tied to power

[1]Centre for Climate Change Research (C3R), Department of Physics, Astronomy and Mathematics, University of Hertfordshire, Hatfield, UK. [2]Department of Civil and Geospatial Engineering, School of Engineering, Newcastle University, Newcastle upon Tyne, UK. [3]Spire Global, Inc., Vienna, Virginia, USA.
✉e-mail: p.r.tiwari@herts.ac.uk

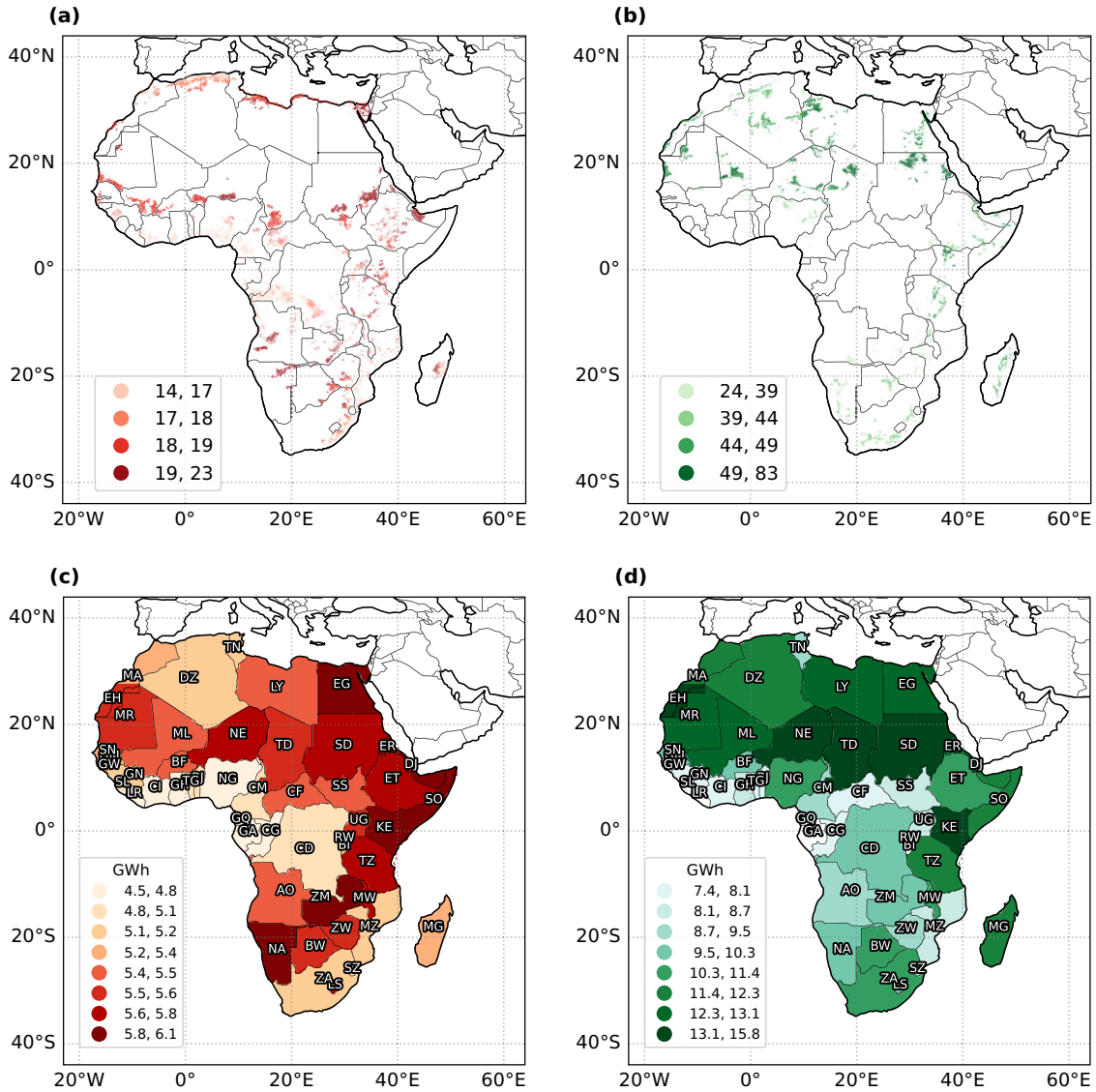

Fig. 1 | Model supply regions (MSRs) and normalized annual yields across Africa. **a** Optimal MSR locations for solar power deployment. **b** Optimal MSR locations for wind power deployment. MSRs are colored by their annual mean capacity factor (CF %). **c** Total annual solar yield (GWh) for each country, normalized by the total MSR area within that country. **d** Total annual wind yield (GWh) for each country, normalized by MSR area.

system impacts. This approach, therefore, offers a promising foundation for developing more accurate operational forecasts for the energy sector.

Despite Africa's centrality to global energy transitions, connections between weather regimes and African RE potential remain underexplored. Existing studies nevertheless reveal influential circulation features, including regimes that organize biomass aerosol transport[24], the modulation of Senegal's conditions by African Easterly Waves[25], links between the Madden–Julian Oscillation and rainfall across southern Africa[26], and circulation patterns associated with South Africa's rainfall variability[27]. Building on these insights, an Africa-focused framework that couples impact-relevant circulation patterns with wind and solar resources mapped onto realistic siting constructs such as MSRs can quantify regime-dependent variability in production and demand and improve sub-seasonal to decadal planning, forecasting, and resilience for the continent's emerging low-carbon power systems.

To optimize country-specific energy generation analysis, we adopt the methodology of Sterl et al[13]., which evaluates renewable resource potential, landuse, population, topography, and infrastructure constraints to identify optimal cost efficient RE deployment sites, termed MSRs. We enhance this approach by incorporating a "variability" criterion for more robust site selection and using a 45-year climatology to strengthen resource potential analysis (see Methods "Datasets"). Energy generation statistics are computed for all countries and analyzed under different scenarios, including climatological conditions and specific weather regimes. Additionally, this study explores links between RE generation and key variability drivers affecting Africa, such as the Madden-Julian Oscillation (MJO)[28], and the El Niño-Southern Oscillation (ENSO)[29] and a novel set of self-organizing maps created based on fields driving RE generation. By identifying regions optimized for cost-efficient and reliable RE deployment and integrating their power generation potential with various large-scale drivers, this study supports Africa's ability to meet its energy demand sustainably and reliably. By identifying key weather patterns associated with maximum variability at MSRs and highlighting the need to improve their predictability, this study presents a pathway toward more reliable and efficient energy forecasting models.

Results

MSRs and climatological annual mean generation

Using the updated MSR creation methodology described in Section "Creating MSRs", we identified optimal locations for solar and wind energy

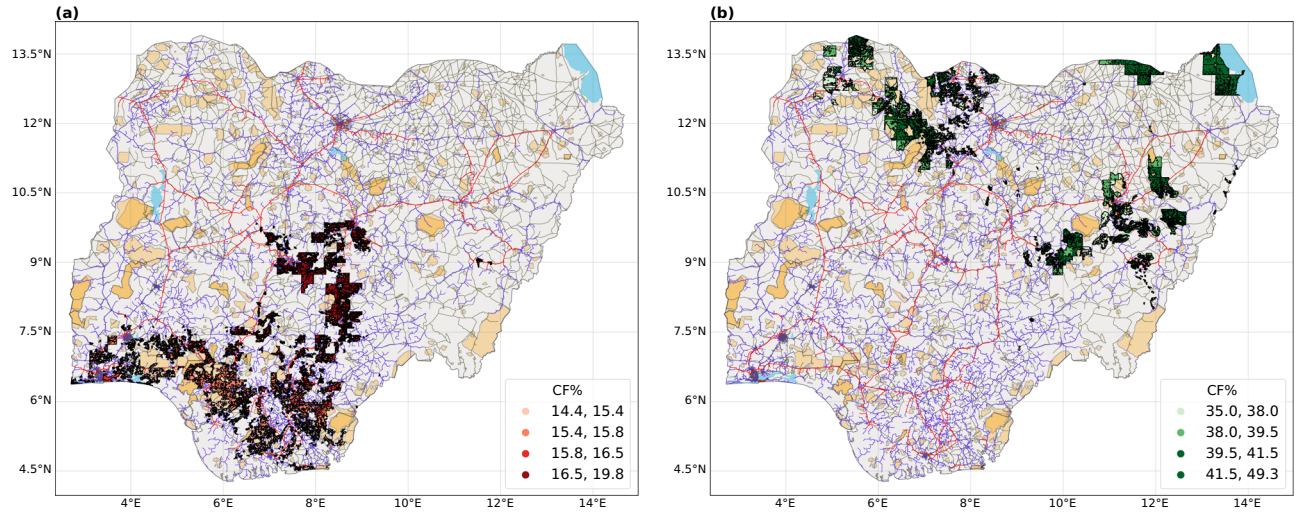

Fig. 2 | Optimal model supply regions (MSRs) for solar and wind deployment in Nigeria. a Locations of solar MSRs, colored by their annual mean Capacity Factor (CF%). **b** Locations of wind MSRs, colored by their annual mean CF%. The maps also show key infrastructure and geographical constraints used in the screening process, including protected areas (orange), water bodies (blue), roads (gray), and transmission (red) and distribution (purple) grids.

deployment across Africa. A spatial map of all screened MSRs is shown in Fig. 1a (solar power) and Fig. 1b (wind power). These MSRs differ from the original work[13] by including variability criteria and 45 years of wind/solar data. While all countries have suitable MSR locations for solar generation, many in central and western Africa lack suitable wind MSRs due to low resource potential. Identified wind MSRs generally have higher mean capacity factors (CF) than solar MSRs. An illustrated map of the MSRs for Nigeria is shown in Fig. 2. The MSR maps of all countries are given in the repository MSRs.

Total annual yields were calculated (See Methods Section "Computing the RE generation statistics from MSRs") for each country using 45 years of weather data. The MSR screening method caps deployment at 5% of a country's total area, giving larger countries higher yields. However, despite their size, Angola and the Democratic Republic of the Congo have lower wind yields due to limited wind resource potential. To emphasize resource potential over country size in total yield, we normalized each country's total annual yield by its total MSR area (Figs. 1c, solar and 1d, wind). Normalized solar power yields are highest in Egypt, Somalia, Kenya, Namibia, Malawi, and Zimbabwe, while wind yields are highest in Kenya, Sudan, Chad, Niger, and Western Sahara.

Weather drivers and clustering analysis

MJO and modulation by ENSO. MJO is a tropical oscillation characterized by an eastward-propagating wave of enhanced (associated with high cloud cover and rainfall) and suppressed convection with a periodicity of 30–60 days[30]. It progresses through eight phases; each linked to distinct convection centers in the tropics (see Methods Section "Identifying MJO phases" for details of the phases and identification methodology). ENSO is a quasi-periodic oscillation (2–7 years) associated with anomalous warming (El Niño) and cooling (La Niña) in the eastern Pacific Ocean[29]. As the dominant source of planetary-scale interannual variability, ENSO impacts global weather through teleconnections[31]. The well-documented modulation of MJO by ENSO[32,33] is the focus of this study, as MJO phases show distinct characteristics during different ENSO modes. Since ENSO varies inter-annually, while MJO is intra-seasonal, we analyze MJO behavior separately for El Niño, La Niña, and neutral years. The ENSO years were identified using the method described in the Methods Section "Identifying El Niño Southern Oscillation (ENSO) modes". Figure 3 presents the Outgoing Longwave Radiation anomaly (OLR) composites of MJO phases for the June-July-August (JJA) season during El Niño and La Niña years. The results for other seasons are in Supplementary information Figs. S2–S4. As ENSO peaks in the boreal winter[29], the MJO anomalies for December-January-February (DJF) are centered in the same DJF season. Due to the lead-lag relation between MJO and ENSO, where MJO activity is enhanced prior to El Niño peaking in winter, with a subsequent weakening of MJO after the peak[34], the MJO anomalies for March-April-May (MAM), June-July-August (JJA), and September-October-November (SON) are considered for the seasons prior to ENSO peak. Comparing anomaly composites of all MJO phases with ENSO modes reveals that El Niño tends to enhance subsidence in MJO phases, while La Niña amplifies convection (Fig. 3). This is evident from the stronger positive OLR anomalies during MJO phases 1, 5, 6, 7, and 8 in El Niño years, indicating enhanced subsidence. Conversely, the negative OLR anomalies during MJO phases 1, 2, 3, and 4 are more pronounced in La Niña years, suggesting stronger convection over the tropical African region.

African OLR regimes. Many regions in Fig. 3 do not exhibit significant anomalies during MJO phases. It is therefore evident that MJO alone cannot account for all fluctuations in the RE system. Taking a similar approach to Bloomfield et al.[23], we wish to create impact-based patterns for potential generation sites. Therefore, we opted for clustering analysis to capture patterns that specifically capture solar radiation variability across the country using OLR fields (focusing particularly on solar due to the large number of identified MSR regions in Fig. 1). This novel approach and its motivation are further explained in the Methods Section "Identifying AORs using clustering analysis". The clustering analysis was performed separately for each of the four seasons, identifying nine prominent weather patterns, hereafter referred to as African OLR regimes (AOR), numbered from 1 to 9. OLR anomaly composite maps for each AOR for season JJA are shown in Fig. 4. The composite maps for all other seasons are provided in the Supplementary Fig. S5. It is evident from Fig. 4 that the spatial OLR anomaly structure in the clustered AORs exhibits distinct complementary patterns, with pairs forming dipole-like structures. This highlights a recurring relationship between contrasting OLR patterns, where one pattern is mirrored by its opposite in both spatial distribution and intensity. For example, the convection centers with strongest anomalies in AOR-1 are flipped in the AOR-2. Similarly, with patterns AOR-3 and 4 and AOR-6 and 9. For AOR 7, the tripolar structures are complemented by AOR-5 and 8. These strongly contrasting patterns are evident across all four seasons. Compared to MJO patterns, the anomaly composites of clustered AORs exhibit stronger

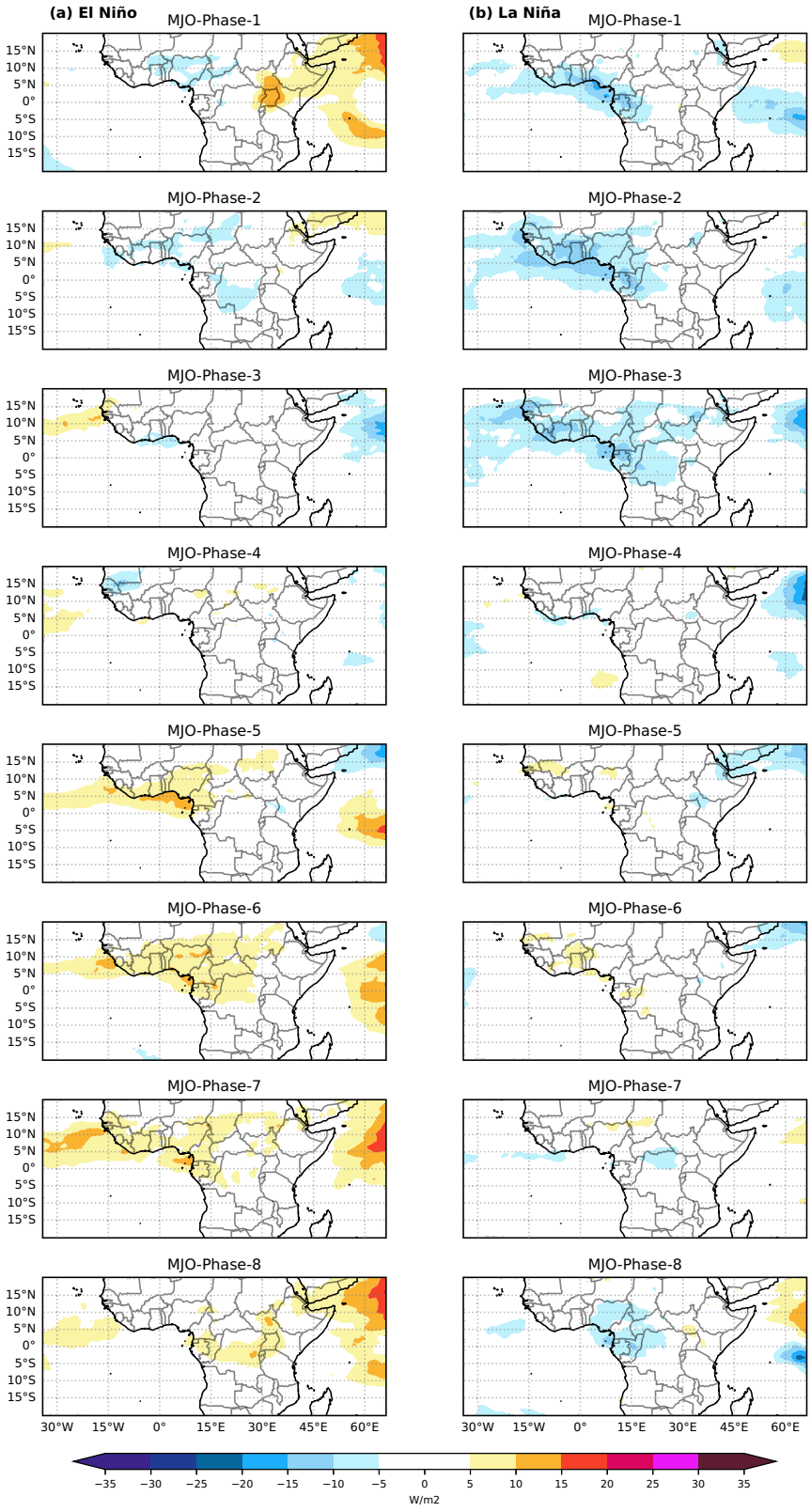

Fig. 3 | OLR anomaly composites for MJO phases during the JJA season, stratified by ENSO state. The figure shows composite maps of Outgoing Longwave Radiation (OLR) anomalies (W/m^2) for each of the eight MJO phases, calculated over the period 1980–2024. **a** Composites for MJO phases during the June-July-August (JJA) season in years preceding an El Niño peak. **b** Composites for MJO phases during the JJA season in years preceding a La Niña peak.

magnitudes, capturing greater weather variability, which in turn could better explain fluctuations in RE generation from the MSRs. Predicting these AORs could greatly aid in forecasting power system variability at sub-seasonal to seasonal (S2S) timescales, as demonstrated over Europe[35]. Some AOR patterns show similar spatial patterns to MJO phases but with higher magnitudes; for example, AOR-1 resembled MJO phase 5, and AOR-4 mirrored MJO phase 6 during JJA. The methodology using Taylor diagrams[36] for the identification of these matching anomaly patterns is presented in the Methods Section "Finding matching patterns between AOR and MJO phases".

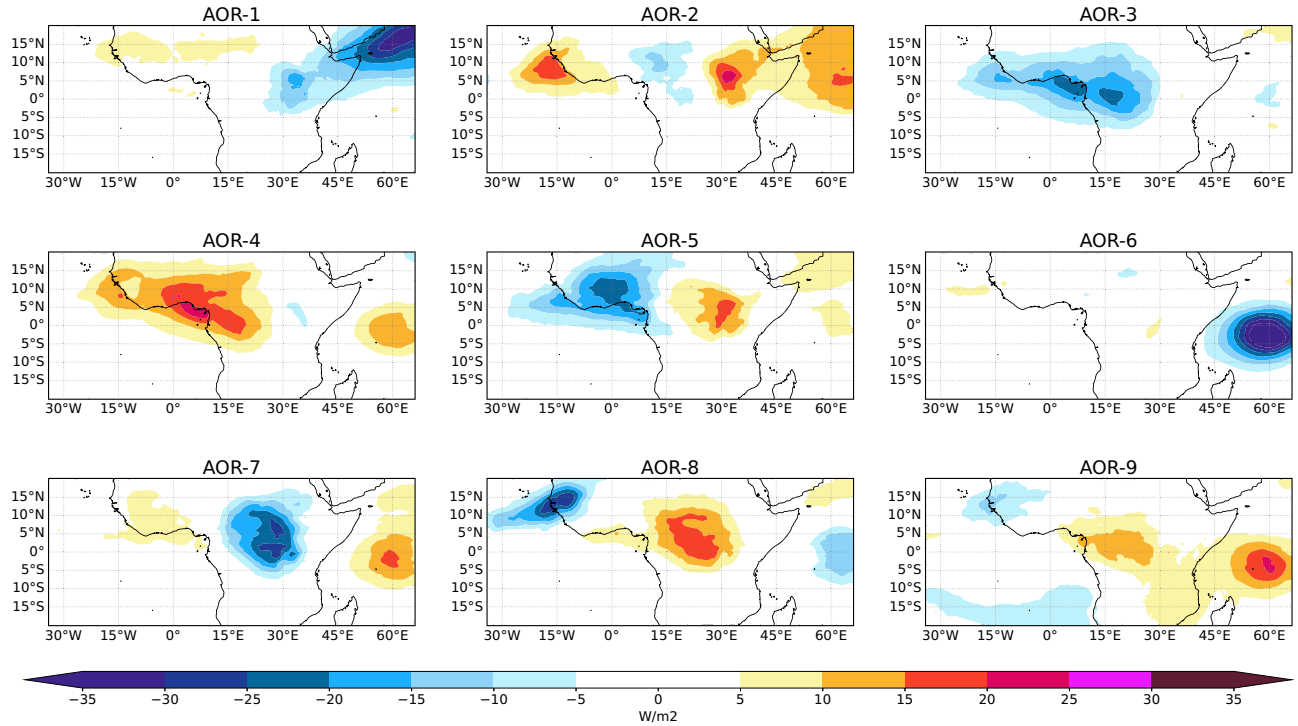

Fig. 4 | OLR anomaly composite maps for the nine African OLR regimes (AORs) during the JJA season. Each panel shows the composite Outgoing Longwave Radiation (OLR) anomaly (W/m2) for one of the nine identified AORs, averaged over all days assigned to that cluster. Negative anomalies (blue regions) indicate enhanced convection, while positive anomalies (red regions) indicate suppressed convection.

Energy generation from MSRs for AORs and MJO

The CF time series and total yield for each AOR day from the MSRs, compared to climatological mean data, are shown for Nigeria (for both solar and wind) in Fig. 5. These were generated as described in the Methods Section "Computing the RE generation statistics from MSRs". It's worth mentioning that for clarity we have shown only the dominant weather patterns in the main figures; full-resolution plots encompassing all patterns across all countries and seasons are available in the repository AOR. For solar power, the diurnal CF cycle remains consistent across regimes, following the climatological pattern. However, CF magnitudes and total daily yields vary. DJF shows the lowest solar generation variability, with yield fluctuations from −6.5% (AOR-8) to +2.6% (AOR-3). In other seasons, RE yield varies significantly across regimes: MAM ranges from −8.4% (AOR-9) to +6.8% (AOR-5), JJA from −8.1% (AOR-4) to +8.5% (AOR-6), and SON from −8.7% (AOR-6) to +6.9% (AOR-2). For wind, the least variability occurs in SON, with yield fluctuations ranging from −9.1% (AOR-6) to +3.5% (AOR-2) compared to climatology. JJA has the largest fluctuations: −16% (AOR-2) and +10.2% (AOR-8). Similarly, the result for MJO during ENSO years is shown in Fig. 6. For solar, MAM exhibits the highest variability, ranging from +8% (phase 6, La Niña) to −6% (phase 1, El Niño). JJA shows the least change (+3.6% in phase 7 La Niña to −4% in phase 8 neutral). Wind RE is more variable overall, with SON showing the largest range (+12% in phase 4 El Niño to −13% in phase 7 La Niña). JJA has the lowest wind variability (+8% in phase 6 neutral to −6% in phase 2 La Niña).

RE generation statistics from MSRs for all countries and seasons, based on MJO phases are available in the repository MJO. As with the AOR analysis, the main figures present a simplified view of the most extreme MJO-ENSO impacts, while the repository contains the full, detailed plots for all combinations. Across all countries, neither AORs nor MJO alone fully explain the largest RE generation variability. In some countries, MJO phases have a stronger impact, while in others, AORs play a more dominant role. To better understand their relative influence, we analyze total yield variability across Africa for all four seasons in a more comprehensive manner. Figure 7 presents the feature associated with maximum and minimum energy yield for solar and wind MSRs in each country during JJA. Distinct regional clustering is observed for solar MSRs, with neighboring countries affected by similar weather patterns. In North Africa, MJO phases predominantly influence both maximum and minimum RE generation, though overall variability is low compared to other regions. In the Sahel, AORs are the primary drivers of RE variability with AOR-4, 7 and 8 causing minimum solar generation while maximum generation is attained during AOR-6. In the western coastal region, AORs 2 and 4 cause minimum yield, and AOR-6 is generally linked to maximum generation. In the Horn of Africa, AOR-9 leads to the lowest generation, with no clear distinction for the feature causing maximum generation. In East Africa, the lowest generation is linked to a mix of MJO phases and AORs, while AOR-3 drives the highest generation. The southern and southwestern regions are also mainly influenced by MJO phases. Overall, variability is highest in tropical regions and lowest in the northern areas. Similar maps for other seasons are provided in Supplementary Figs. S7–S9.

Wind MSRs show significantly higher RE generation fluctuations than solar MSRs. Similar to solar, clustering of similar features causing minimum and maximum generation can be observed in wind energy production. The northern Africa variability is associated with MJO phases. In the western African region, AOR-2 widely causes a minimum in wind generation while maximum is associated with different features. The variability in generation in the horn of Africa region is predominantly influenced by MJO phases with phase 1 during El Niño years tend to have minimum generation, but maximum is associated with different phases. The variability in southern African region is driven by a mix of AORs and MJO phases. The region encompassing Uganda, Kenya, South Sudan, and the Central African Republic is of particular interest as it exhibits the highest variability in wind generation. Notably, Uganda experiences a 53% above-normal generation during AOR-5, while MJO phase-4 (under neutral ENSO) results in a 25% decline. This analysis highlights the significant influence of weather regimes and MJO phases on RE generation, revealing distinct regional drivers of MSR yield variability. These findings provide a basis for understanding energy

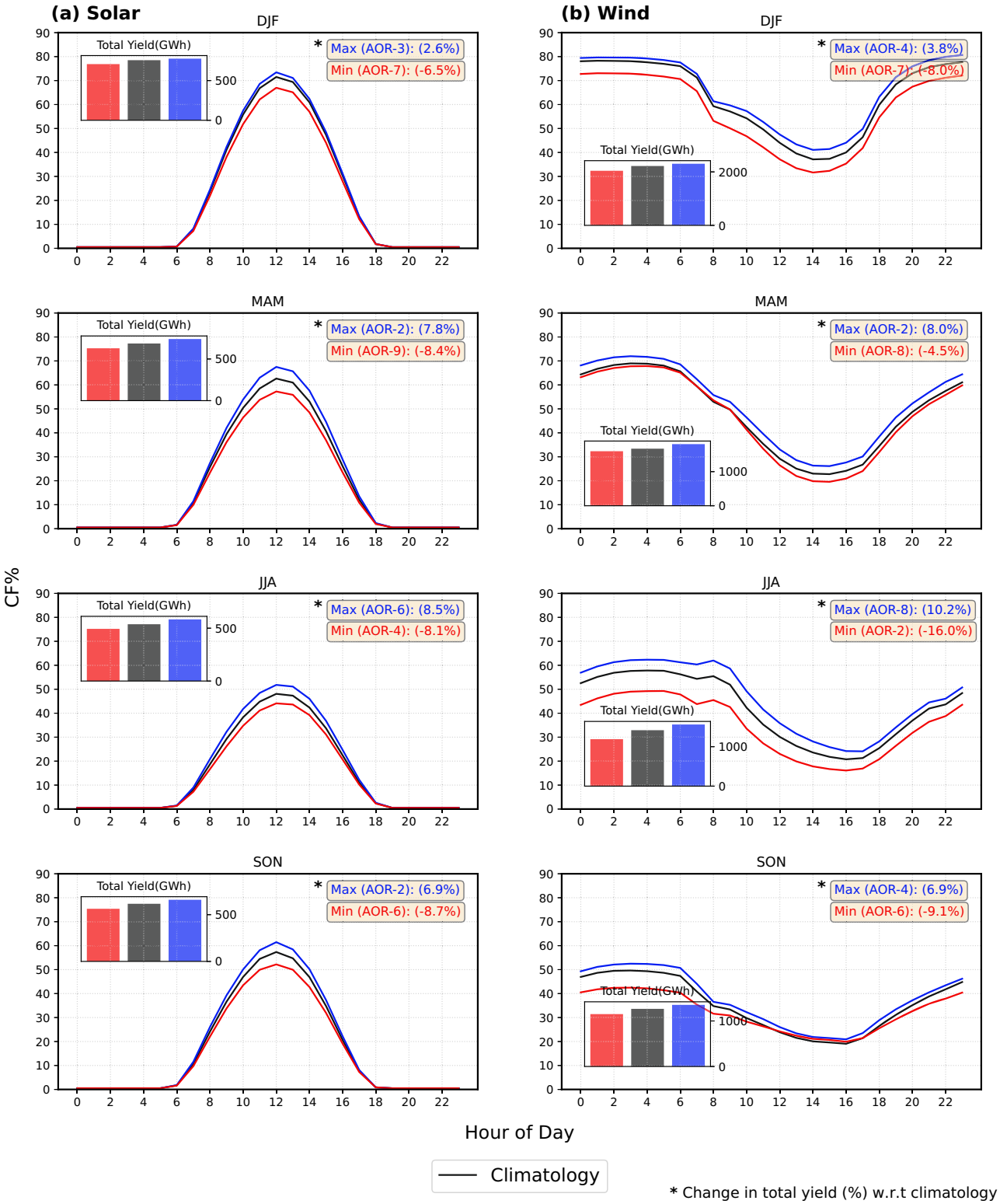

Fig. 5 | Impact of African OLR regimes (AORs) on renewable energy generation in Nigeria. The figure shows the mean diurnal cycles of the capacity factor (CF) for **a** solar and **b** wind, averaged across all Nigerian MSRs for each season. For each season, the plot displays the climatological mean diurnal cycle (black line) alongside the cycles for the AORs that produce the maximum (blue line) and minimum (red line) total daily yields. Inset bar charts show the total daily yield (GWh) for these three cases. The text boxes identify the specific AORs responsible for the maximum and minimum yields and their percentage deviation from climatology.

fluctuations, aiding RE deployment and planning under different synoptic conditions, and a starting point for sub-seasonal prediction system development.

Discussion

This study presents a detailed and refined approach for optimizing RE deployment across continental Africa. We present an updated MSR list for

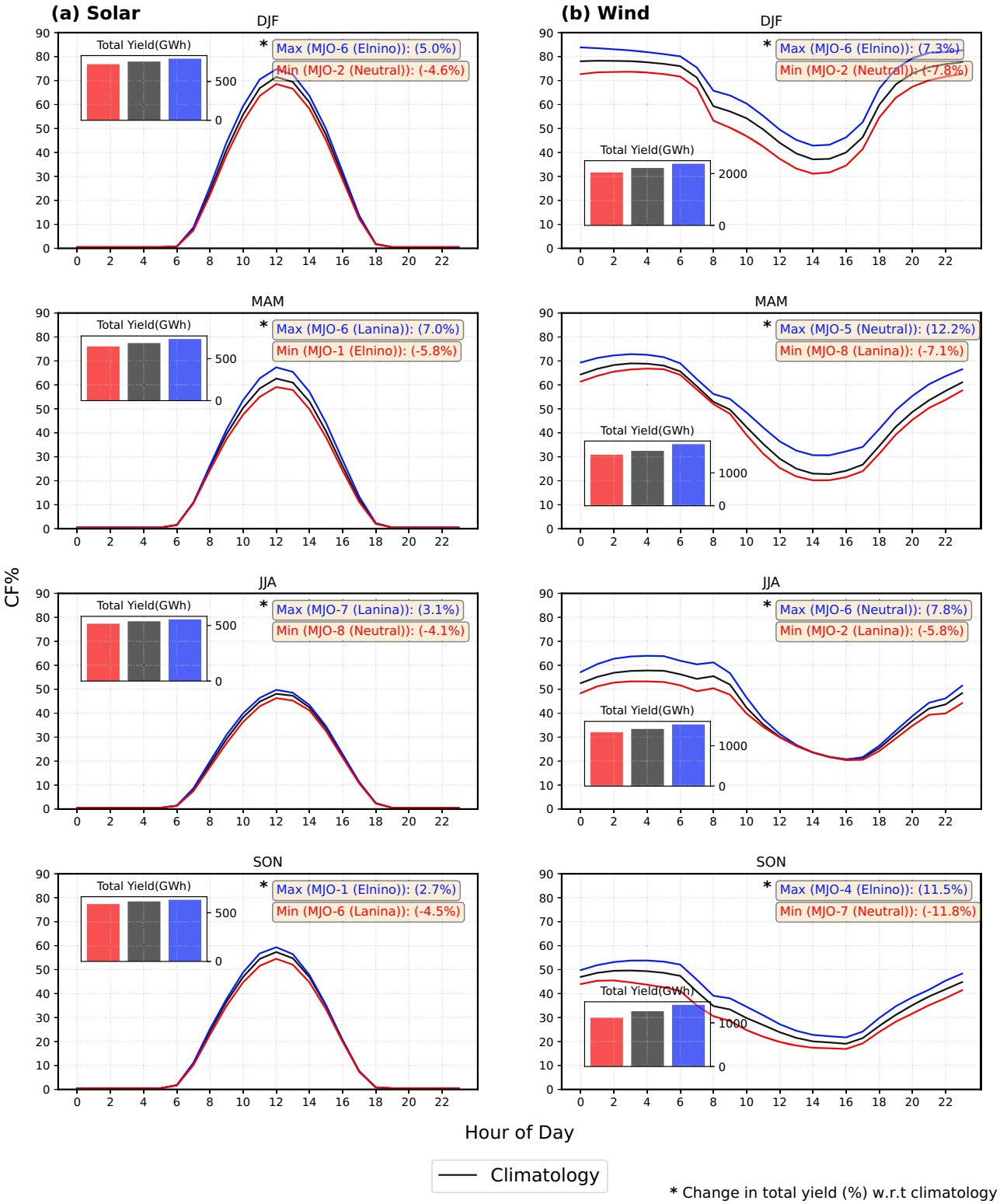

Fig. 6 | Impact of MJO-ENSO combinations on renewable energy generation in Nigeria. The figure shows the mean diurnal cycles of the capacity factor (CF) for **a** solar and **b** wind, averaged across all Nigerian MSRs for each season. For each season, the plot displays the climatological mean diurnal cycle (black line) alongside the cycles for the MJO-ENSO combinations that produce the maximum (blue line) and minimum (red line) total daily yields. Inset bar charts show the total daily yield (GWh) for these three cases. The text boxes identify the specific MJO-ENSO combinations responsible for the maximum and minimum yields and their percentage deviation from climatology.

each African country, factoring in meteorological variability and long-term data for cost-efficient, reliable RE generation. We then analyzed RE generation variability from these MSRs under MJO phases during different ENSO modes and a novel set of regimes called AORs. These OLR-derived AORs revealed higher anomaly magnitudes than traditional MJO anomalies across Africa, better representing system variabilities than traditional weather patterns. The RE yield from these MSRs was subsequently computed for climatological scenarios and specific MJO phases/AORs across all

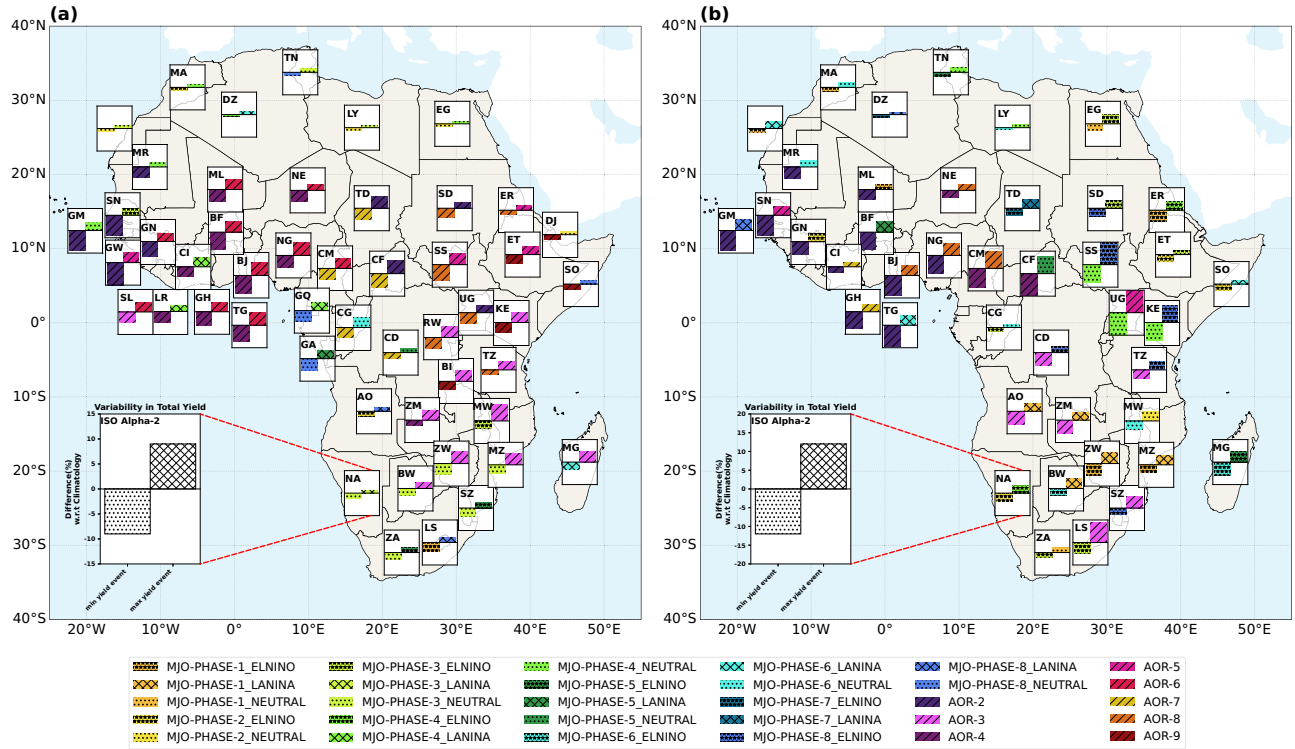

Fig. 7 | Weather features associated with maximum and minimum renewable energy yields during the JJA season. The maps show the specific weather feature that causes the largest positive (maximum) and negative (minimum) deviation in total yield from the climatological mean for **a** solar and **b** wind. Each country is marked with a symbol representing the feature associated with the minimum yield (left bar) and maximum yield (right bar). The color and hatch pattern for each feature (AORs and MJO-ENSO combinations) are defined in the main legend at the bottom. The inset graph provides a larger, representative example of a country's yield variability, showing the percentage deviation from the mean.

four seasons. Our analysis reveals significant regional disparities in RE generation potential. During JJA, West and Central African solar MSRs show maximum variability, with AORs 2 and 4 yielding least (occurring for 7 and 9 days per season, respectively), and AOR-6 yielding most RE production (increasing solar yield by 8% and occurring for 16 days). This region being frequented by the West African monsoon[37] and African easterly waves, may explain the enhanced variability, potentially captured by our AORs. An additional cluster of high solar variability is observed in southeastern Africa during JJA, where MJO phase 3 during neutral ENSO years (occurring for 15 days) and AOR-3 (with an expected frequency of 7 days per season) dominate the variability. Considering other seasons, DJF saw maximum variability in East Africa, the Horn of Africa, and southeastern Africa, and MAM in central Africa and the East African monsoon domain. The highest variability during SON is found to be scattered across the continent. The least variability in solar is found in North Africa.

Overall, the variability from wind MSRs is very high compared to solar MSRs. Among all the countries, Uganda stands out with exceptionally high variability in wind generation throughout the year. The Central-East African region generally displays high wind generation variability across all seasons. For example, in East Africa during JJA, MJO phase 8 during El Niño is associated with the highest RE generation (occurring for 11 days), while MJO phase 4 during a neutral ENSO year adversely affects wind generation (occurring for 9 days). The least variability in wind generation is found in north and northwest Africa. Frequency of occurrence of each weather feature is shown in Fig. 8. Accurate forecasting of weather patterns in MSRs is crucial for both daily RE operations and long-term planning, enabling early warnings and effective preparedness for reliable RE deployment across Africa. By quantifying RE yield from MSRs under different synoptic weather conditions, this work establishes a robust framework for weather aware RE deployment, underscoring the significance of understanding and predicting these patterns across timescales to optimize RE generation. A key implication is the potential for S2S forecasting using our novel AORs. Our Africa-centric AORs better explain local energy variability because, unlike the globally-defined MJO, they capture regional weather patterns that are often missed in large-scale composites. The prospects for their S2S predictability are promising. Since the MJO has known predictive skill in the S2S models on these timescales[38], the AORs that resemble MJO phases are therefore likely to inherit this forecast skill. The predictability of the other, more regional AORs, however, remains an open question and a new forecasting challenge. Therefore, a crucial next step is to conduct the first formal predictability assessment of all AORs. Such an analysis would be essential not only for quantifying their forecast skill but also for diagnosing the diverse physical drivers from global teleconnections to regional processes that govern these impact-relevant weather regimes.

Methods

Datasets

This study employs the European Centre for Medium-Range Weather Forecasts (ECMWF) Reanalysis version 5 (ERA5) dataset[39] to calculate renewable potentials across Africa. ERA5 provides comprehensive, globally consistent high-resolution data, making it a suitable choice for analyzing meteorological and climatic variables in regions where ground-based observations are sparse or unavailable, such as in many parts of Africa. By combining model simulations and observations through data assimilation, ERA5 provides reliable reconstructions of the past weather and their validity as proxy for observations is well documented in literature[40–42]. The variables used in this study are: Wind speed (at 100 m above ground), temperature (at 2 m above ground), and surface solar radiation downwards at the surface for calculating renewable energy outputs; outgoing longwave radiation (OLR) for AOR and MJO phase identification; and sea surface temperature (SST) and mean sea level pressure (MSLP) for ENSO identification. Hourly data was utilized except for ENSO identification, where monthly fields were

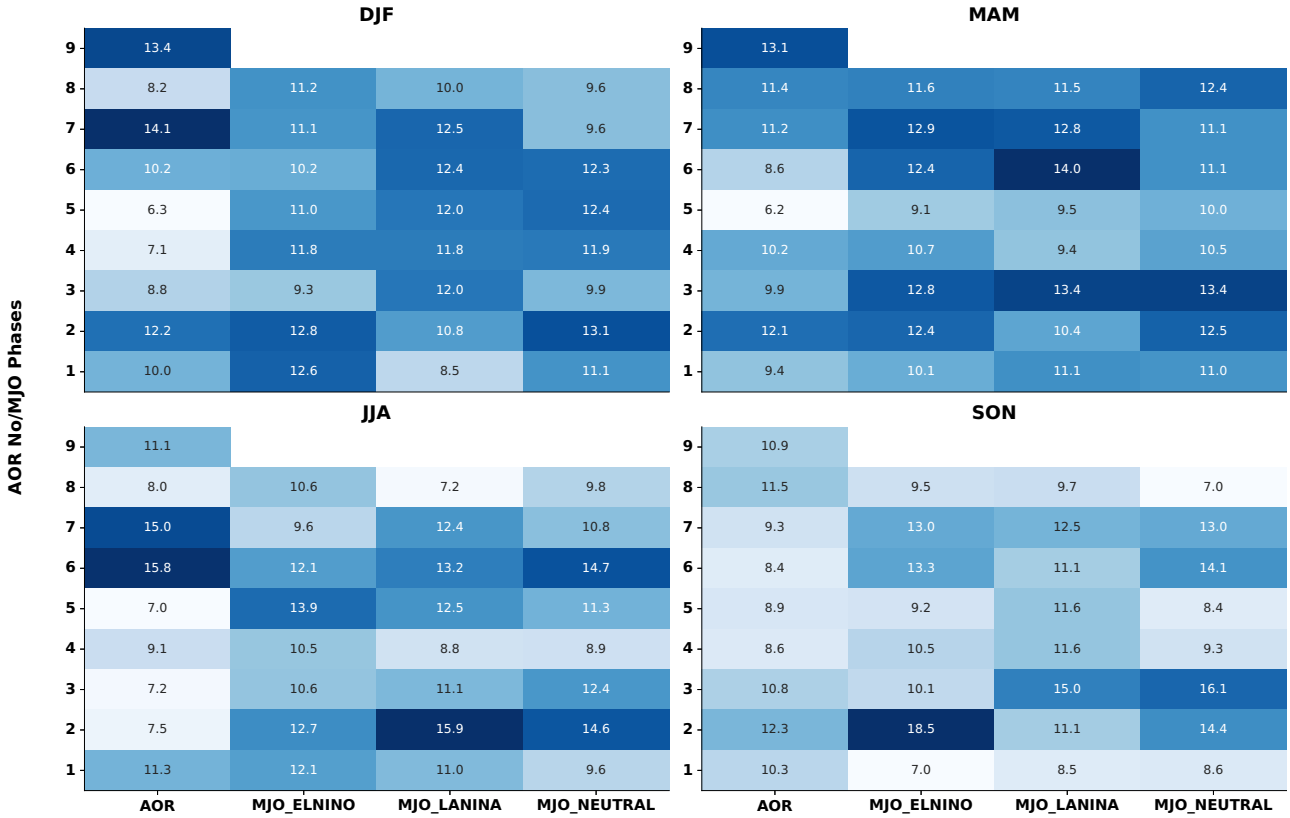

Fig. 8 | Mean occurrence frequency of AORs and MJO phases. The four heatmaps show the mean number of occurrence days per season for each identified weather feature, averaged over the 1980–2024 period. The y-axis represents the nine AORs and eight MJO phases, while the *x*-axis shows the AORs and MJO phases further stratified by ENSO state (El Niño, La Niña, and Neutral).

employed. All datasets span the period from 1980 to 2024. The static datasets for MSR identification can be found in Sterl et al.[13]. To account for systemic biases in the ERA5 reanalysis, we corrected the data using the high-resolution Global Solar Atlas (GSA)[43] and Global Wind Atlas (GWA)[44] as a reference. For each grid point, we calculated an additive offset from the difference between the long-term mean of the reference atlas and the raw ERA5 data, and then added this constant offset to the entire 45-year hourly ERA5 time series. This mean adjustment method ensures that the long-term climatology of our input data matches the reference atlases. It is also important to note that our results are presented as deviations from the climatological state, making our conclusions about the relative impact of different weather patterns unaffected by any constant mean bias in the energy yield time series.

Creating MSRs

The methodology for identifying MSRs is adapted from Sterl et al.[13] to determine optimal locations for solar and wind deployment across Africa, using the following criteria: For resource potential, solar regions with climatologically average Global Horizontal Irradiance (GHI) < 4 kWh/m²/day and wind regions with wind speeds <6 m/s at 100 m height were excluded. Locations with population density >100 inhabitants/km², elevation >2000 meters above sea level, and slope >20% were excluded. Land use was limited to specific categories from the European Space Agency (ESA) Globe Cover map, while protected areas (from the World Database on Protected Areas) were excluded. Only regions within 50 km of existing roads and power grids were considered. After creating this first set of MSRs, hourly CFs for solar and wind were calculated using ERA5 data for 2018, and Levelized Cost of Electricity (LCOE) was computed for each MSR. Later MSRs with the lowest LCOE were selected, ensuring their total area did not exceed 5% of the country's total land area.

In contrast to the original[13] MSRs, which were only calculated with a single year of weather data, we recreated them using a climatological year, based on the mean of 45 years of GHI and wind data (1980–2024) from ERA5. We also incorporated variability of solar and wind resources into the screening criteria, as high variability affects the financing of new renewable generation[14]. The standard deviation of hourly GHI and 100-m wind speed was calculated at each of the MSRs and used as the variability index (VAR). The LCOE and VAR were then normalized and added together by giving 75% weight to LCOE and 25% weight to VAR to create the combined LCOE-VAR index. The weighting criterion for the combined LCOE-VAR index was determined through experimentation, viewing the balance as a trade-off between economic optimization (lowest LCOE) and operational reliability (lowest VAR). We started with a 100% weight on LCOE and gradually increased the weight given to variability. We found that when the weight for VAR exceeded 25%, the selected MSRs no longer substantially overlapped with the regions having the highest resource potential (i.e., those identified by the 100% LCOE approach). Because of this, the 75–25% balance was chosen for our index as it represents a scenario that strongly favors economic potential while still giving a tangible consideration for grid stability. This framework is inherently flexible. For instance, planners with different priorities could increase the weight of variability to 40% or 50%, placing a higher premium on a stable energy supply. Such a change would likely alter MSR site selection by favoring regions with more consistent, even if less powerful, renewable resources. The weighting thus acts as a tuneable parameter, allowing site selection to be aligned with specific national or regional policy goals.

Computing the RE generation statistics from MSRs

Each MSR's rated power-generating capacity is determined by its area and plant specifications. The actual energy generated is obtained by multiplying

Table 1 | IEC Wind Turbine classification and corresponding wind speeds

IEC class	Wind speed
Class 3	< 7.5 m/s
Class 2	7.5–8.5 m/s
Class 1	>8.5 m/s

hourly CFs by the MSR's rated power. Following the methodology in Sterl et al.[13], we assume that not the entire area from each MSR is allocated for power generation, as space is required for infrastructure, such as on-site roads. Consequently, 90% of the MSR area is designated for solar power generation, while 75% is allocated for wind energy. To study the impact of AORs and MJO on RE generation from MSRs, the hourly CFs for all days corresponding to specific regimes and MJO phases (ENSO modes separately) were calculated using the methodology described in Sections "Solar power model" and "Wind Power model". The mean diurnal cycle of CFs for a typical regime/MJO phase day at each MSR was determined by averaging the CF for each hour across all days within that AOR/MJO phase. This diurnal CF time series was generated for each MSR in every African country across all four seasons. Additionally, the total daily yield for each AOR/MJO phase was calculated. To assess country-level impacts, the mean CF across all MSRs within each country was computed, and the total generation was determined by summing the total yield from all MSRs within the country. For comparison purposes, the power generation for climatological mean days is also calculated.

Solar power model

The parameter used to evaluate solar energy potential is the solar photovoltaic (Solar PV) CF. CF, expressed as a percentage, is defined as the ratio of the actual energy produced by a solar power plant to its theoretical maximum output under standard environmental conditions.

The energy generated by a Solar PV system depends on the downward shortwave radiation flux, commonly known as Global Horizontal Irradiation (GHI), as well as the ambient temperature (T2M). The formula for calculating the Solar PV CF is adapted from Bloomfield et al.[12] and is given by:

$$\mathrm{SolarPVCF}(t) = \frac{ActualSolarPVOutput}{SolarPVOutputunderStandardConditions} = \eta * \frac{G(t)}{G_{STC}} \quad (1)$$

Where:

- $G(t)$: is the incoming global horizontal irradiance (GHI) at each hour in W/m².
- G_{STC}: is the reference irradiance under standard test conditions (STC), a constant of 1000 W/m².
- η: is the *relative efficiency* of the solar panel.

This *relative efficiency* term models the panel's real-world performance by accounting for the decrease in cell efficiency per unit increase in the ambient temperature. It is defined as:

$$\eta = 0.9 \times (1 - 0.0042 \times (T_{2m} - T_{ref})) \quad (2)$$

This efficiency term has two components.

- *Temperature-dependent efficiency*: The term $1 - 0.0042 \times (T_{2m} - T_{ref})$ calculates the dynamic change in the panel's performance based on its temperature. This factor decreases the efficiency when the ambient temperature (T_{2m}) is above the 25 °C (T_{ref}) reference and increases it when the temperature is below 25 °C. It is the primary variable factor affecting the panel's hour-to-hour performance.
- *Static loss factor*: This is the constant 0.9 in the formula, and it accounts for all the non-weather-related losses, applying a baseline 10% performance penalty.

Wind power model

The Wind CF is defined as the ratio of a wind turbine's actual power output to its maximum rated power output. A standard hub height of 100 m is used for wind turbines, and the power curve of a turbine is applied to convert wind speed at this height into the Wind Power CF. This methodology is adapted from Bloomfield et al.[12]. Instead of relying on a single turbine class to compute the wind CF, we consider three different classes of wind turbines, categorized according to the International Electrotechnical Commission (IEC) classification[45]. Based on the mean wind speed over a given grid cell, the corresponding IEC turbine class is assigned to that location, and the appropriate power curve is used to determine the Wind CF for that grid cell. The IEC classification of wind turbines is outlined in Table 1.

Identifying MJO and ENSO

The methods of identifying MJO and ENSO modes were adopted from literature and the detailed methodologies are given below. The analysis was carried out for all African countries for four climatological seasons, DJF, MAM, JJA, and SON.

Identifying El Niño Southern Oscillation (ENSO) modes. El Niño and La Niña years were identified using the method outlined in AchutaRao et al.[46], based on both the NINO3 and SOI indices. The NINO3 index is the area-averaged monthly SST anomaly in the NINO3 region (5°N–5°S and 150°W–90°W) and SOI (Southern Oscillation Index) is measured as the difference in sea level pressure anomalies between Tahiti and Darwin (Australia). An El Niño year is defined as one where the standardized NINO3 index is greater than 0.6 and the standardized SOI is less than −0.6 during the DJF season. Conversely, a La Niña year is identified when the standardized NINO3 index is less than −0.6 and the standardized SOI is greater than 0.6.

Identifying MJO phases. MJO exhibits 8 phases. In phase 1, convection is strongest over the western Indian Ocean, gradually shifting eastward until phase 8, where an MJO cycle terminates in the central Pacific and the next cycle begins[47]. This study uses an Outgoing Longwave Radiation (OLR)-Based MJO index (OMI) first developed by Kiladis et al.[48] and made into an easy-to-use Python package called "mjoindices" by Hoffmann et al.[49]. The first two principal components (PC1 & PC2) of OLR form the MJO index. The PCs are computed by projecting 20–96 day filtered OLR onto the EOF patterns of 30–96 day eastward filtered OLR. A Wheeler-Hendon phase diagram[47] can then be used to find out the phase of the MJO. The phase diagram can be visualized as a scatter graph plotted between PC1 and PC2 values. The graph is divided into eight sectors corresponding to each phase of the MJO. The sector where the PC1 value meets PC2 is the phase of the MJO. An objective implementation of the phase diagram method, written in Python, is used for identifying the MJO phases from the MJO index. After identifying the MJO phases, seasonal OLR anomaly composites for the period 1980–2024 were computed using daily OLR maps for each phase across the tropical African region (20°S–20°N, 35°W–65°E) for the seasons DJF, MAM, JJA, and SON. This tropical African domain, encompassing both the African continent and adjacent parts of the Atlantic and Indian Oceans, was chosen to capture the convective anomalies associated with the MJO phases where it is active. OLR anomaly composites are used to visualize MJO phases as they depict enhanced (negative OLR anomalies indicating convection) and suppressed (positive OLR anomalies indicating reduced cloudiness) convection associated with the different phases of MJO. The anomaly composites are presented in Supplementary Fig. S1. These composites show different convection and subsidence centers, indicated by negative and positive OLR anomalies, respectively. To assess MJO-ENSO teleconnections, MJO phases were grouped separately by each ENSO mode, and seasonal OLR anomaly composites were computed. Since ENSO peaks in DJF, DJF composites are centered on the same ENSO year, while those for MAM, JJA, and SON correspond to seasons leading up to ENSO's peak.

Identifying AORs using clustering analysis

To identify weather regimes over Africa, we use the Self-Organizing Maps (SOM) algorithm, a clustering method based on artificial neural networks[50]. In SOM, a map of neurons is initialized with random weights, and a Best Matching Unit (BMU) is selected based on the least distance measure between input vectors and neurons. The neuron weights are then adapted towards the input vectors using a learning rate, and the process repeats over multiple iterations until each input vector is assigned to a BMU. For clustering, we use the Python implementation of the SOM algorithm called MiniSom[51].

Major weather variabilities over the Tropical African region include the Madden-Julian Oscillation (MJO)[30], African Easterly Waves (AEW)[52], and Equatorial Kelvin and Rossby Waves[53], each with different periodicities (30–60 days for MJO[30], 3–5 and 6–9 days for AEW[52], 3–20 days for Kelvin Waves[53] and 10–72 days for Rossby waves[53]). To capture these variabilities, we focused on the tropical African belt, setting the domain for clustering between 35°W–65°E and 20°N–20°S, an area dominated by these weather events. As these target features are linked to convection and subsidence, outgoing longwave radiation (OLR) data were used as a proxy for convective activity, with negative OLR anomalies indicating enhanced convection and positive anomalies indicating subsidence. To exclude unwanted frequencies such as low-frequency seasonal variations and high-frequency day-to-day changes, we applied a bandpass filter to remove periodicities greater than 100 days and less than 3 days. Finally, SOM with a 3×3 node shape was applied to the bandpass filtered daily OLR anomaly data, identifying 9 distinct weather regimes called African OLR regimes (AOR) over the study area. Deciding the number of SOM nodes was done after doing some experimentation. Initially, we experimented with SOM configurations from 2×2, gradually increasing the size to 2×3, 2×4, 3×3, 3×4, and 4×4. We observed that as the number of nodes increased, identifying a clear "elbow" in the quantization error for objective cluster selection became difficult. Because increasing the number of clusters can lead to overfitting and redundant patterns that are difficult to interpret, we determined the number of clusters subjectively. Our decision to use a 3×3 configuration considered the frequency of occurrence of the resulting patterns, which is important for sub-seasonal to seasonal (S2S) forecasting, and their spatial pattern similarity to existing phenomena such as the MJO. Details of assessing the pattern similarity with MJO can be found in Section "Finding matching patterns between AOR and MJO phases".

Finding matching patterns between AOR and MJO phases

Taylor diagrams[36] were created between each clustered AOR and the MJO phase patterns to find out if the clustered regimes showed similarity to MJO phases. The similarity between two patterns, measured by the correlation between two patterns, their root-mean-square difference, and the individual amplitude of variations (measured using the individual standard deviations), can be graphically illustrated using a Taylor diagram. Using the statistics observed from the Taylor diagrams, the patterns with the least RMSE and highest correlation coefficient are chosen as the closest matching patterns, and they are plotted together to see how the AORs and MJO phases resemble each other and a sample matching patterns are shown in Supplementary Fig. S6.

Data availability

The ERA5 reanalysis data used in this study are publicly available from the Copernicus Climate Change Service (C3S) Climate Data Store. The derived numerical data supporting the findings of this study, such as the final MSR shapefiles and processed yield statistics, are available from the corresponding author upon request. A full repository containing all supplementary figures generated for every African country (including individual MSR maps and yield plots) is publicly available on GitHub [repo](https://github.com/rajeevskurup/msr_aor_re_figures).

Code availability

The custom codes used to perform the analysis and generate the figures are available from the corresponding author upon reasonable request.

Received: 5 June 2025; Accepted: 5 January 2026;
Published online: 02 February 2026

References

1. Wu, G. C., Deshmukh, R., Ndhlukula, K., Radojicic, T. & Reilly, J. *Renewable Energy Zones for the Africa Clean Energy Corridor*. LBNL--187271 Rev., 1328753 https://doi.org/10.2172/1328753 (2015).
2. Cáceres, A. L., Jaramillo, P., Matthews, H. S., Samaras, C. & Nijssen, B. Potential hydropower contribution to mitigate climate risk and build resilience in Africa. *Nat. Clim. Chang.* **12**, 719–727 (2022).
3. Jones-Albertus, R. et al. Solar on the rise: how cost declines and grid integration shape solar's growth potential in the United States. *MRS Energy Sustain.* **5**, E4 (2018).
4. Mallapragada, D. S., Diaz Pilas, D., Gonzalez Fernandez, P. & Delgado Martín, A. *System Implications of Continued Cost Declines for Wind and Solar on Driving Power Sector Decarbonization*. https://dspace.mit.edu/handle/1721.1/130576 (2020).
5. IEA. *Clean Energy Investment for Development in Africa* (IEA, 2024).
6. Peters, R. et al. Sustainable pathways towards universal renewable electricity access in Africa. *Nat. Rev. Earth Environ.* **5**, 137–151 (2024).
7. Welsch, M. et al. Smart and just grids for sub-Saharan Africa: exploring options. *Renew. Sustain. Energy Rev.* **20**, 336–352 (2013).
8. Hafner, M., Tagliapietra, S. & de Strasser, L. Prospects for renewable energy in Africa. in (eds Hafner, M., Tagliapietra, S. & de Strasser, L) *Energy in Africa: Challenges and Opportunities*, 47–75 (Springer International Publishing, 2018).
9. Prăvălie, R., Patriche, C. & Bandoc, G. Spatial assessment of solar energy potential at global scale. A geographical approach. *J. Clean. Prod.* **209**, 692–721 (2019).
10. Dajuma, A. et al. Sensitivity of solar photovoltaic panel efficiency to weather and dust over West Africa: comparative experimental study between Niamey (Niger) and Abidjan (Côte d'Ivoire). *Comput. Water Energy Environ. Eng.* **5**, 123–147 (2016).
11. Mentis, D., Hermann, S., Howells, M., Welsch, M. & Siyal, S. H. Assessing the technical wind energy potential in Africa a GIS-based approach. *Renew. Energy* **83**, 110–125 (2015).
12. Bloomfield, H. C., Wainwright, C. M. & Mitchell, N. Characterizing the variability and meteorological drivers of wind power and solar power generation over Africa. *Meteorol. Appl.* **29**, e2093 (2022).
13. Sterl, S. et al. An all-Africa dataset of energy model "supply regions" for solar photovoltaic and wind power. *Sci. Data* **9**, 664 (2022).
14. Sinsel, S. R., Riemke, R. L. & Hoffmann, V. H. Challenges and solution technologies for the integration of variable renewable energy sources —a review. *Renew. Energy* **145**, 2271–2285 (2020).
15. Bremen, L. V. Large-scale variability of weather dependent renewable energy sources. in (ed. Troccoli, A.) *Management of Weather and Climate Risk in the Energy Industry*, 189–206 (Springer Netherlands, 2010).
16. Widén, J. et al. Variability assessment and forecasting of renewables: a review for solar, wind, wave and tidal resources. *Renew. Sustain. Energy Rev.* **44**, 356–375 (2015).
17. Wiel, K. vander et al. The influence of weather regimes on European renewable energy production and demand. *Environ. Res. Lett.* **14**, 094010 (2019).
18. Cassou, C. Intraseasonal interaction between the Madden–Julian oscillation and the North Atlantic oscillation. *Nature* **455**, 523–527 (2008).
19. Liu, Y., Feng, S., Qian, Y., Huang, H. & Berg, L. K. How do North American weather regimes drive wind energy at the sub-seasonal to seasonal timescales? *npj Clim. Atmos. Sci.* **6**, 1–10 (2023).
20. Pozo-Vazquez, D., Santos-Alamillos, F. J., Lara-Fanego, V., Ruiz-Arias, J. A. & Tovar-Pescador, J. The impact of the NAO on the solar and wind energy resources in the Mediterranean Area. in (eds Vicente-Serrano, S. M. & Trigo, R. M.) *Hydrological, Socioeconomic and Ecological Impacts of the North Atlantic Oscillation in the Mediterranean Region*, 213–231 (Springer Netherlands, 2011).

21. Ely, C. R., Brayshaw, D. J., Methven, J., Cox, J. & Pearce, O. Implications of the North Atlantic oscillation for a UK–Norway renewable power system. *Energy Policy* **62**, 1420–1427 (2013).
22. François, B. Influence of winter North-Atlantic oscillation on climate-related-energy penetration in Europe. *Renew. Energy* **99**, 602–613 (2016).
23. Bloomfield, H. C., Brayshaw, D. J. & Charlton-Perez, A. J. Characterizing the winter meteorological drivers of the European electricity system using targeted circulation types. *Meteorol. Appl.* **27**, e1858 (2020).
24. Gaetani, M. et al. A weather regime characterisation of winter biomass aerosol transport from southern Africa. *Atmos. Chem. Phys.* **21**, 16575–16591 (2021).
25. Guèye, A. K. et al. Weather regimes over Senegal during the summer monsoon season using self-organizing maps and hierarchical ascendant classification. Part I: synoptic time scale. *Clim. Dyn.* **36**, 1–18 (2011).
26. Oettli, P., Tozuka, T., Izumo, T., Engelbrecht, F. A. & Yamagata, T. The self-organizing map, a new approach to apprehend the Madden–Julian oscillation influence on the intraseasonal variability of rainfall in the southern African region. *Clim. Dyn.* **43**, 1557–1573 (2014).
27. Wolski, P., Jack, C., Tadross, M., van Aardenne, L. & Lennard, C. Interannual rainfall variability and SOM-based circulation classification. *Clim. Dyn.* **50**, 479–492 (2018).
28. Madden, R. A. & Julian, P. R. Detection of a 40–50 day oscillation in the zonal wind in the Tropical Pacific. *J. Atmos. Sci.* **28**, 702–708 (1971).
29. Philander, S. G. H. El Niño and La Niña. *J. Atmos. Sci.* **42**, 2652–2662 (1985).
30. Zhang, C. Madden-Julian Oscillation. *Rev. Geophys.* **43**, RG2003 (2005).
31. McPhaden, M. J., Zebiak, S. E. & Glantz, M. H. ENSO as an integrating concept in Earth science. *Science* **314**, 1740–1745 (2006).
32. Moon, J.-Y., Wang, B. & Ha, K.-J. ENSO regulation of MJO teleconnection. *Clim. Dyn.* **37**, 1133–1149 (2011).
33. Dasgupta, P., Roxy, M. K., Chattopadhyay, R., Naidu, C. V. & Metya, A. Interannual variability of the frequency of MJO phases and its association with two types of ENSO. *Sci. Rep.* **11**, 11541 (2021).
34. Hendon, H. H., Wheeler, M. C. & Zhang, C. Seasonal dependence of the MJO–ENSO relationship. *J. Clim.* **20**, 531–543 (2007).
35. Bloomfield, H. C., Brayshaw, D. J., Gonzalez, P. L. M. & Charlton-Perez, A. Pattern-based conditioning enhances sub-seasonal prediction skill of European national energy variables. *Meteorol. Appl.* **28**, e2018 (2021).
36. Taylor, K. E. Summarizing multiple aspects of model performance in a single diagram. *J. Geophys. Res. Atmos.* **106**, 7183–7192 (2001).
37. Froidurot, S. & Diedhiou, A. Characteristics of wet and dry spells in the West African monsoon system. *Atmos. Sci. Lett.* **18**, 125–131 (2017).
38. Vitart, F. Madden—Julian Oscillation prediction and teleconnections in the S2S database. *Q. J. R. Meteorol. Soc.* **143**, 2210–2220 (2017).
39. Hersbach, H. et al. The ERA5 global reanalysis. *Q. J. R. Meteorol. Soc.* **146**, 1999–2049 (2020).
40. Gleixner, S., Demissie, T. & Diro, G. T. Did ERA5 improve temperature and precipitation reanalysis over East Africa? *Atmosphere* **11**, 996 (2020).
41. Steinkopf, J. & Engelbrecht, F. Verification of ERA5 and ERA-Interim precipitation over Africa at intra-annual and interannual timescales. *Atmos. Res.* **280**, 106427 (2022).
42. King, J. A., Engelstaedter, S., Washington, R. & Munday, C. Variability of the Turkana low-level jet in reanalysis and models: implications for rainfall. *J. Geophys. Res. Atmos.* **126**, e2020JD034154 (2021).
43. World Bank Group. *Global Solar Atlas*. at https://globalsolaratlas.info/ (2024).
44. Davis, N. N. et al. The Global Wind Atlas: a high-resolution dataset of climatologies and associated web-based application. *Bull. Am. Meteorol. Soc.* **104**, E1507–E1525 (2023).
45. International Electrotechnical Commission. Wind energy generation systems – Part 1: Design requirements. IEC 61400-1:2019. Geneva: IEC, (2019).
46. AchutaRao, K. & Sperber, K. Simulation of the El Niño Southern oscillation: results from the Coupled Model Intercomparison Project. *Clim. Dyn.* **19**, 191–209 (2002).
47. Wheeler, M. C. & Hendon, H. H. An All-season Real-time Multivariate MJO Index: development of an Index for Monitoring and Prediction. *Mon. Weather Rev.* **132**, 1917–1932 (2004).
48. Kiladis, G. N. et al. A comparison of OLR and circulation-based indices for tracking the MJO. *Mon. Weather Rev.* **142**, 1697–1715 (2014).
49. Hoffmann, C. G., Kiladis, G. N., Gehne, M. & von Savigny, C. A Python package to calculate the OLR-Based Index of the Madden- Julian-oscillation (OMI) in climate science and weather forecasting. *J. Open Res. Softw.* **9**, 9 (2021).
50. Kohonen, T. Self-organized formation of topologically correct feature maps. *Biol. Cybern.* **43**, 59–69 (1982).
51. Vettigli, G. MiniSom: minimalistic and NumPy-based implementation of the Self Organizing Map. *GitHub*. https://github.com/JustGlowing/minisom (2018).
52. Diedhiou, A., Janicot, S., Viltard, A. & de Felice, P. Evidence of two regimes of easterly waves over West Africa and the tropical Atlantic. *Geophys. Res. Lett.* **25**, 2805–2808 (1998).
53. Knippertz, P. et al. The intricacies of identifying equatorial waves. *Q. J. R. Meteorol. Soc.* **148**, 2814–2852 (2022).

Acknowledgements

We first thank both the reviewers for their constructive comments that helped improving the quality of the paper. This research was supported by the C3R/PAM studentship to RSK at the University of Hertfordshire. We thank Dr James L Collett for his valuable feedback and for language polishing and grammatical correction.

Author contributions

All authors contributed to the design of the study. R.S.K. carried out the main work under the supervision of P.R.T., H.B., N.A., and E.H. R.S.K. wrote the software code, collected the data, and conducted the data analysis. All authors contributed to writing the manuscript.

Competing interests

The authors declare no competing interests.

Additional information

Supplementary information The online version contains supplementary material available at https://doi.org/10.1038/s44406-026-00019-7.

Correspondence and requests for materials should be addressed to P. R. Tiwari.